Materials Transactions, Vol. 60, No. 9 (2019) pp. 1763 to 1768
Special Issue on Latest Research and Development of Structural and Functional Titanium-Based Materials

Effects of Fe on Microstructures and Mechanical Properties of Ti–15Nb–25Zr–(0, 2, 4, 8)Fe Alloys Prepared by Spark Plasma Sintering

Qiang Li[1,*], Xufeng Yuan[1], Junjie Li[2], Pan Wang[3], Masaaki Nakai[4], Mitsuo Niinomi[1,5,6,7,*], Takayoshi Nakano[6], Akihiko Chiba[5], Xuyan Liu[1] and Deng Pan[8,9]

[1]*School of Mechanical Engineering, University of Shanghai for Science and Technology, Shanghai 200093, P. R. China*
[2]*International Iberian Nanotechnology Laboratory (INL), Av. Mestre José Veiga, Braga 4715-330, Portugal*
[3]*Singapore Institute of Manufacturing Technology, 73 Nanyang Drive, 637662, Singapore*
[4]*Department of Mechanical Engineering, Faculty of Science and Engineering, Kindai University, Higashiosaka 577-8502, Japan*
[5]*Institute for Materials Research, Tohoku University, Sendai 980-5377, Japan*
[6]*Department of Materials and Manufacturing Science, Graduate School of Engineering, Osaka University, Suita 565-0871, Japan*
[7]*Department of Materials Science and Engineering, Graduate School of Science and Technology, Meijo University, Nagoya 468-8502, Japan*
[8]*Materials Genome Institute, Shanghai University, Shanghai 200444, China*
[9]*Research Center for Advanced Metallic Materials, Yangtze Delta Region Institute of Tsinghua University, 705 Yatai Road, Jiaxing, Zhejiang, China*

Biomedical Ti–15Nb–25Zr–(0, 2, 4, 8)Fe (mol%) alloys are prepared by mixing pure element powders and spark plasma sintering (SPS). Specimens with diameters of 20 mm and thicknesses of 3 mm are obtained by sintering at 1000°C for 10 min followed by cooling in the furnace. Some of the specimens are then heat-treated at 900°C for 1 h followed by water quenching. Zr and Fe are dissolved in Ti; however, segregation of Nb is observed in all of the alloys. The β and α'' phases are observed in the as-sintered and heat-treated specimens owing to the insufficient diffusion of the alloying elements. Fe stabilizes the β phase and provides a solution-strengthening effect. With the increase in the Fe content in the as-sintered specimen, the compressive strength and micro-Vickers hardness are improved in the Ti–15Nb–25Zr–(0, 2, 4)Fe alloys and slightly decreased in Ti–15Nb–25Zr–8Fe. The as-sintered Ti–15Nb–25Zr–4Fe alloy exhibits the maximum compressive strength of 1740 MPa. Although the plasticity is decreased by the Fe addition, a fracture strain of approximately 17% is obtained for Ti–15Nb–25Zr–4Fe, indicating a good plasticity. The heat treatment cannot eliminate the segregation of Nb, but can improve the plasticity and slightly increase the strengths of Ti–15Nb–25Zr–(0, 2, 4)Fe. Moreover, the heat-treated Ti–15Nb–25Zr–8Fe exhibits a high strength of approximately 1780 MPa and fracture strain of approximately 19%. Therefore, good comprehensive mechanical properties, including high strengths, high hardnesses, and good plasticities, can be obtained in Fe-added β-Ti alloys prepared by SPS and subsequent optional short heat treatment. [doi:10.2320/matertrans.ME201913]

(Received January 29, 2019; Accepted March 29, 2019; Published May 24, 2019)

Keywords: *spark plasma sintering, Ti alloy, compression, Fe*

1. Introduction

Compared with the traditional stainless steel and Co–Cr–Mo alloys, Ti and Ti alloys have been extensively used for ideal implant materials in biomedical devices, particularly for artificial implant materials, owing to their unique properties including low densities, high specific strengths, low Young's moduli, superior corrosion resistances, and excellent biocompatibilities.[1–3] As Al and V are toxic and allergy-causing elements, the Ti–6Al–4V extra-low interstitial (ELI, mass%), which is a typical material for implant applications, was considered to cause damage to the body.[4,5] Recently, a series of β-type titanium alloys have been developed by adding Nb, Zr, Mo, Ta, and Sn. These elements are nontoxic and thus do not cause adverse reactions in the human body.[6–9] Zr and Nb have large atomic radii and high solid solubilities in Ti alloys.[10] Recently, Ti–Nb–Zr alloys have attracted significant attention owing to their combination of high strengths and low moduli of elasticity, and thus are regarded as one of the most promising biomaterials.[11–14] Various Ti–Nb–Zr alloys were recently developed such as Ti–10Nb–20Zr (mol%, hereafter, the chemical compositions of the alloys are expressed in mol%),[15] Ti–28Nb–35.4Zr,[16] and Ti–24Nb–(0, 2, 4)Zr.[17]

The melting method is usually used to fabricate Ti alloys followed by thermal and mechanical processing to obtain certain shapes and desirable properties.[18] Waste of materials is produced during the reducing material processing. The traditional powder metallurgy method needs a prolonged high-temperature sintering, which usually causes excessive oxidization and grain coarsening, leading to poor properties.[19–21] Spark plasma sintering (SPS) is a new powder sintering technology. It has many advantages, such as simple operation, low sintering temperature, high heating and cooling rates, short sintering time, clean preparation process, and optimization of material structure, which substantially improve the mechanical properties of the sintered bulk.[22–24] Although it's considered that the O content in the sintered specimen is usually higher than that of melted one, the O can significantly increase the strength. The spark plasma sintered Ti–35Nb–7Zr–5Ta (mass%) alloy with O content around 0.36 mass% (around 1.4 mol%) performs the compressive fracture strength higher than 1300 MPa.[25] Moreover, the compressive fracture strength of the Ti–26Nb–5Ag alloy prepared by SPS is approximately three times that of the conventional vacuum-sintered alloy,[26] indicating the advantage of SPS. The Ti–20Nb–13Zr alloy prepared by SPS consists of the β, α, and α'' phases and exhibits a high micro-Vickers hardness above 600 HV.[27] Thus, it's believed that SPS is appropriate method to prepare bulk β-Ti alloys with high performance.

*Corresponding authors, E-mail: jxli@tju.edu.cn, liqiang@usst.edu.cn; niinomi@imr.tohoku.ac.jp

Fe is a low-cost and low-melting-point element. It is an effective β stabilizer in β-Ti and can enhance the mechanical properties of the Ti alloys.[28] The Ti–5Ag–xFe alloys has been confirmed no cytotoxicity and exhibit excellent biocompatibility,[29] therefore, it's believed that Fe can be used to develop biomedical Ti alloys. In this study, the Nb content is set to 15 mol% to avoid excessive segregations. Considering the influences of Nb and Zr on β transus in the Ti–Nb and Ti–Zr binary phase diagrams,[30] the Zr content is raised to 25 mol% to obtain metastable β phase at room temperature. Fe was added to obtain increased β stability, high strengths and good plasticities of the Ti–15Nb–25Zr alloys prepared by SPS.

2. Experimental Procedure

Pure Ti, Nb, Zr, and Fe powders with purities of 99.9% were used as raw materials. The powders with a nominal composition of Ti–15Nb–25Zr–(0, 2, 4, 8)Fe (mol%) were mixed for 12 h in a V-type mixing machine at a speed of 120 r/min. The blended powders were put into a graphite mold with a diameter of 20 mm, and then placed in SPS equipment. A thin graphite foil was used between the powders and interior surfaces of the graphite mold to reduce the friction and facilitate the extraction of the sintered sample. Air evacuation and argon refilling were carried out three times in the furnace before the sintering. The final gas pressure was below 5 Pa. The graphite mold with the powders was heated at a rate of 100°C/min until the sintering temperature of 1000°C. They were then cooled inside the furnace to room temperature after holding for 10 min at the sintering temperature. The axial pressure was set to 50 MPa and continuously applied during the heating and cooling processes. The obtained samples had diameters of 20 mm and thicknesses of 3 mm. Rectangular specimens with sizes of 3 mm × 3 mm × 6 mm were cut using an electric discharging machine for subsequent measurements. Some samples were further heat-treated at 900°C for 1 h followed by water quenching.

The phase compositions were analyzed by X-ray diffraction (XRD) with Cu K_α radiation at a voltage of 40 kV, current of 40 mA, and scanning speed of 6°/min. The specimens were ground, polished, and etched in a 2-vol% HF solution for 10 s to observe the optical microstructures. The chemical compositions were characterized by a field-emission scanning electron microscope (SEM) equipped with an energy-dispersive spectrometer (EDS). Compression tests were carried out at room temperature using an electronic universal testing machine with a cross-head speed of 1 mm/min. The Vickers hardness was measured using a Mitutoyo MH–140 tester with a load of 19.61 N (2000 gf) and dwell time of 10 s. Ten points were measured for each specimen.

3. Results and Discussion

3.1 Phase composition

The sintering temperature of 1000°C is higher than the β transus temperature of pure Ti; therefore, Zr, Nb, and Fe can be dissolved in the β phase of Ti during the sintering. The XRD spectra (Fig. 1) show that the β phase is the main phase in Ti–15Nb–25Zr–(0, 2, 4, 8)Fe. This indicates that Zr, Nb, and Fe are dissolved in Ti. In addition, weak diffraction peaks of the α'' phase can be observed in all of the four alloys owing to the metastable β phase. However, diffraction peaks of Fe–Ti (FeTi) and Fe–Zr (Fe_2Zr) intermetallic compounds are observed in Ti–15Nb–25Zr–8Fe. This indicates that Fe is not well distributed in Ti. With the increase in the Fe content, the diffraction peaks of the β phase slightly shift to higher angles, as Fe with its smaller atomic radius decreases the lattice parameters of the β phase.

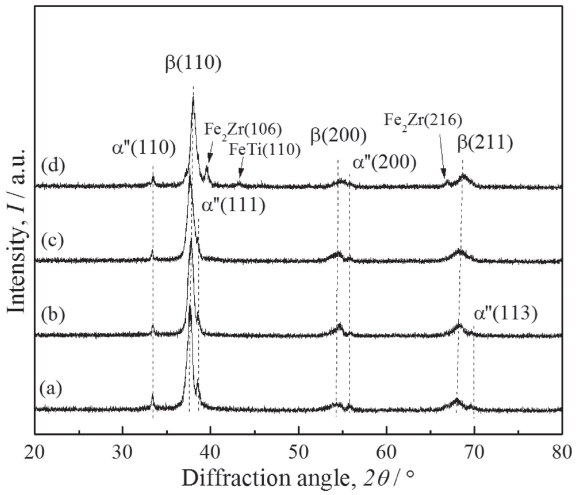

Fig. 1 XRD patterns of the as-sintered Ti–15Nb–25Zr–(0, 2, 4, 8)Fe: (a) Ti–15Nb–25Zr, (b) Ti–15Nb–25Zr–2Fe, (c) Ti–15Nb–25Zr–4Fe, and (d) Ti–15Nb–25Zr–8Fe.

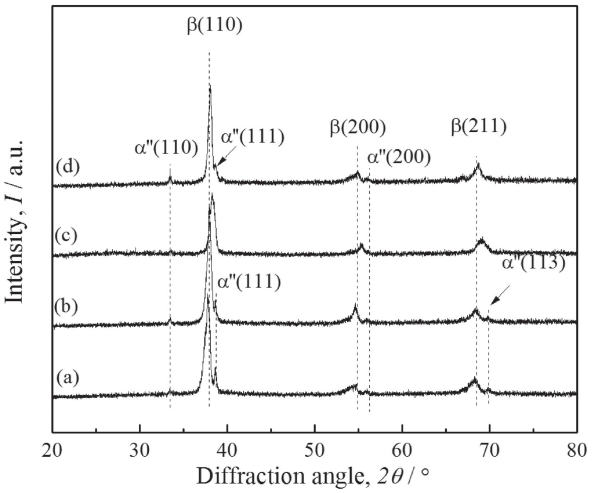

Fig. 2 XRD patterns of Ti–15Nb–25Zr–(0, 2, 4, 8)Fe subjected to the heat treatment at 900°C for 1 h: (a) Ti–15Nb–25Zr, (b) Ti–15Nb–25Zr–2Fe, (c) Ti–15Nb–25Zr–4Fe, and (d) Ti–15Nb–25Zr–8Fe.

The peaks corresponding to the α'' phase in Ti–15Nb–25Zr–(0, 2, 4, 8)Fe are weaker after the heat treatment (Fig. 2). The peaks of the intermetallic compounds in Ti–15Nb–25Zr–8Fe disappear and Ti–15Nb–25Zr–4Fe exhibits almost single β phase. The XRD results indicate that the heat treatment causes further diffusion of Zr, Nb, and Fe in the β phase of the alloy and increases the β phase stability.

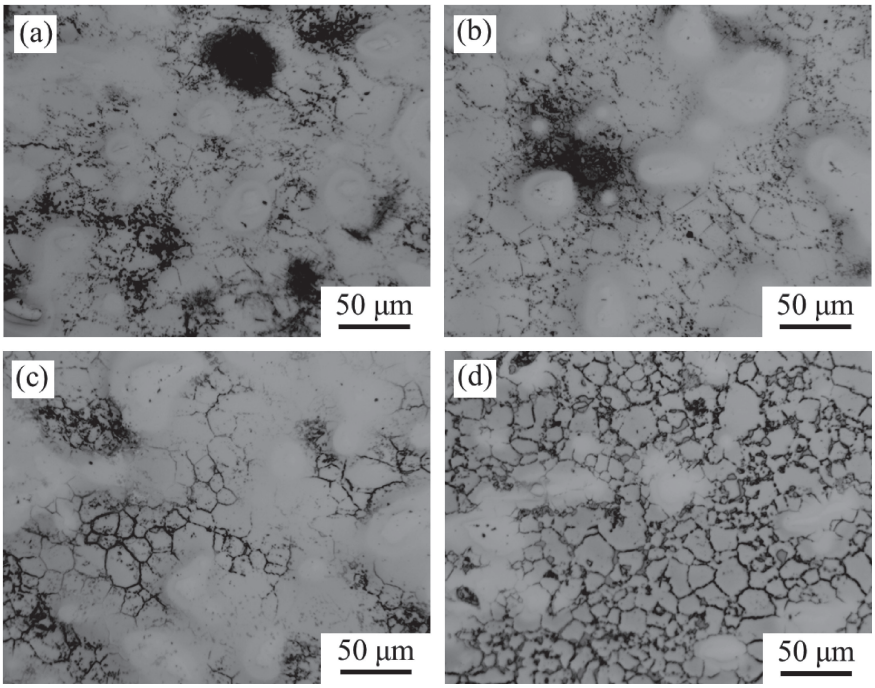

Fig. 3 Optical micrographs of the as-sintered Ti–15Nb–25Zr–(0, 2, 4, 8)Fe: (a) Ti–15Nb–25Zr, (b) Ti–15Nb–25Zr–2Fe, (c) Ti–15Nb–25Zr–4Fe, and (d) Ti–15Nb–25Zr–8Fe.

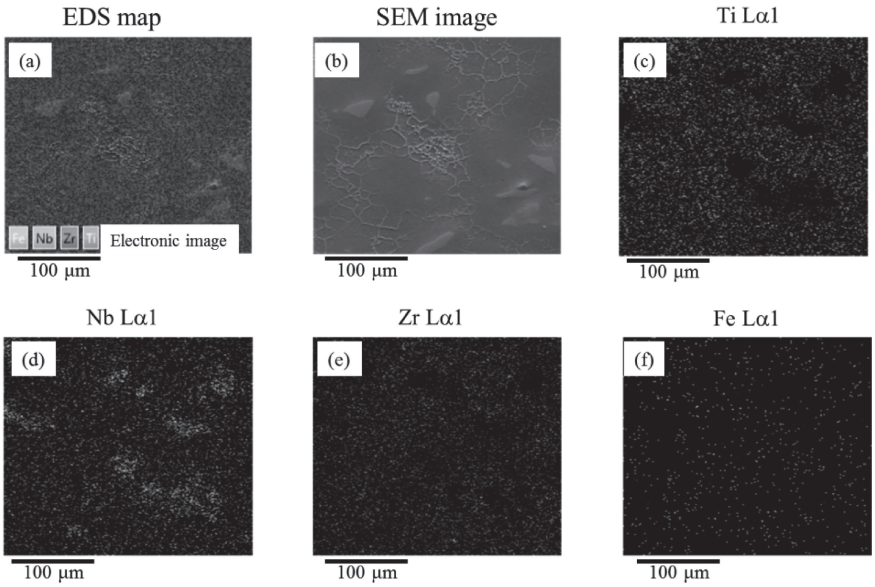

Fig. 4 EDS mapping of the element distributions in the as-sintered Ti–15Nb–25Zr–(0, 2, 4, 8)Fe: (a) element map, (b) SEM image, and (c) Ti, (d) Nb, (e) Zr, and (f) Fe maps.

3.2 Microstructure

The optical microstructures of the as-sintered Ti–15Nb–25Zr–(0, 2, 4, 8)Fe alloys consist of black, gray, and bright white regions, as shown in Fig. 3. The black parts are grain boundaries and overetched parts. The gray part has the largest area and is supposed to be the β phase. The intermetallic compounds and α'' phase are hardly observed from the optical microstructure considering their minor quantities. The grain boundaries are hardly observed in Ti–15Nb–25Zr, but become clear with the increase in the Fe content. According to the EDS results in Fig. 4, the bright white region corresponds to segregation of Nb. Nb has a high melting temperature and lower diffusion speed; therefore, some large Nb powder particles cannot be fully dissolved in the β phase. The segregation cannot be easily detected by XRD, as Nb exhibits a diffraction peak at the same position as that of β-Ti in the XRD pattern. The segregation of Nb explains the metastability of the β phase in Ti–15Nb–25Zr–(0, 2, 4, 8)Fe. The β grains become more obvious with the increase in the Fe content, while the bright white regions become slightly smaller. Fe is beneficial to the formation of β grains.

After the heat treatment, decrease in the bright white area and increase in the gray area are observed for all of the alloys with clearer β grains, as shown in Fig. 5. This indicates that the heat treatment causes further diffusion of alloying elements. However, the segregation of Nb is not eliminated,

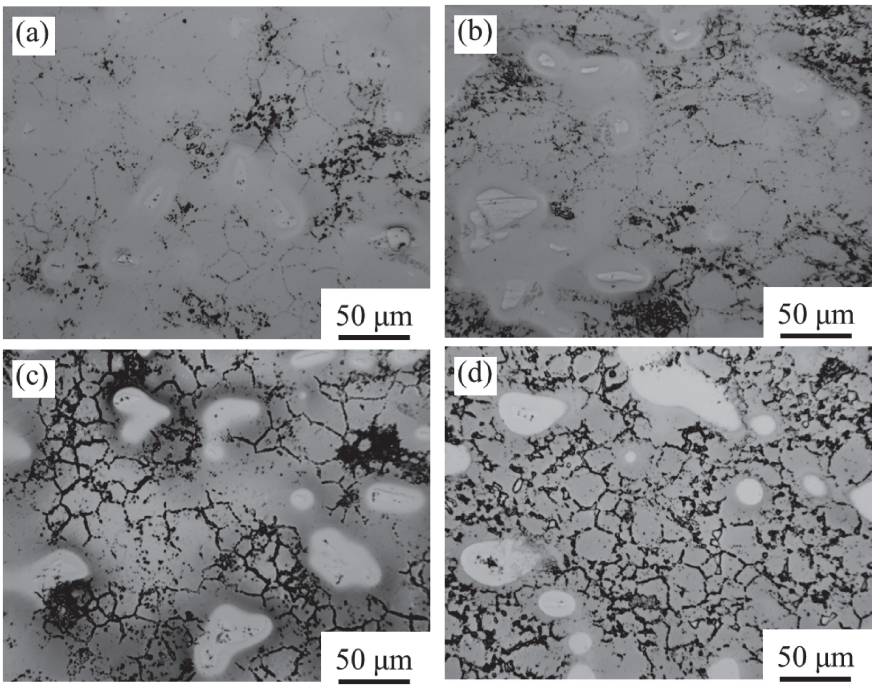

Fig. 5 Optical micrographs of Ti–15Nb–25Zr–(0, 2, 4, 8)Fe subjected to the heat treatment at 900°C for 1 h: (a) Ti–15Nb–25Zr, (b) Ti–15Nb–25Zr–2Fe, (c) Ti–15Nb–25Zr–4Fe, and (d) Ti–15Nb–25Zr–8Fe.

according to the bright white area clearly observed in the optical microstructure. The short heat treatment provides only a limited improvement in elemental distribution.

3.3 Micro-Vickers hardness

All of the specimens exhibit large deviations in micro-Vickers hardness of approximately ±20 HV owing to the insufficient diffusion of raw element powders and segregation of Nb, as shown in Fig. 6. The as-sintered Ti–15Nb–25Zr exhibits a high micro-Vickers hardness up to 350 HV. The micro-Vickers hardness increases with the Fe content in the range of 0% to 4 mol%, indicating that Fe provides a solid-solution strengthening effect. However, the micro-Vickers hardness of Ti–15Nb–25Zr–8Fe is not higher than that of Ti–15Nb–25Zr–4Fe. Considering the XRD and microstructural results, the larger content of Fe does not dissolve into the matrix and forms intermetallic compounds such as FeTi and Fe_2Zr, reducing the amounts of other constitutional elements such as Nb and Zr in the matrix and leading to a reduced solid-solution strengthening. The precipitation hardening effects by FeTi and Fe_2Zr may be canceled to some extent by the reduction in the solid-solution strengthening by the reduction in the amounts of dissolved Nb and Zr caused by the addition of a large amount of Fe.

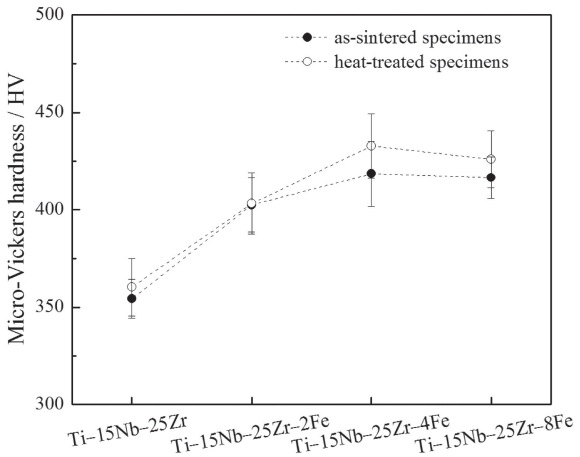

Fig. 6 Micro-Vickers hardnesses of the as-sintered and heat-treated Ti–15Nb–25Zr–(0, 2, 4, 8)Fe.

The micro-Vickers hardness is only slightly increased in the heat-treated Ti–15Nb–25Zr–(0, 2, 4)Fe mainly owing to the small increase in the solid-solution effect. For Ti–15Nb–25Zr–8Fe, the increase in micro-Vickers hardness is due to the solid-solution hardening caused by the dissolution of FeTi and Fe_2Zr in the matrix.

3.4 Compressive mechanical properties

Figure 7 shows compressive stress–strain curves of Ti–15Nb–25Zr–(0, 2, 4, 8)Fe before and after the heat treatment. Figure 8 shows the compressive strength, σ_b, and 0.2% proof stress, $\sigma_{0.2}$, obtained by compressive tests. The as-sintered Ti–15Nb–25Zr–(0, 2, 4, 8)Fe exhibit similar trends in σ_b and $\sigma_{0.2}$ with the increase in the Fe content to those of the micro-Vickers hardness. σ_b of Ti–15Nb–25Zr is 1470 MPa, which increases up to approximately 1740 MPa at an Fe content of 4 mol% (Ti–15Nb–25Zr–4Fe). At an Fe content of 8 mol% (Ti–15Nb–25Zr–8Fe), σ_b decreases to 1670 MPa. The decrease can be attributed to the insufficient diffusion of the alloying elements, as suggested by the XRD and microstructure results, which implies a reduced solid-solution effect, as discussed above. All of the specimens exhibit relatively large plastic deformations before breaking. The region in each compressive stress–strain curve after the yielding (i.e., 0.2% proof stress) strain (compressive elastic strain) to the fracture strain, where the increasing stress is retarded, is defined as stress plateau. The stress plateau reflects the plasticity of the specimen. According to the

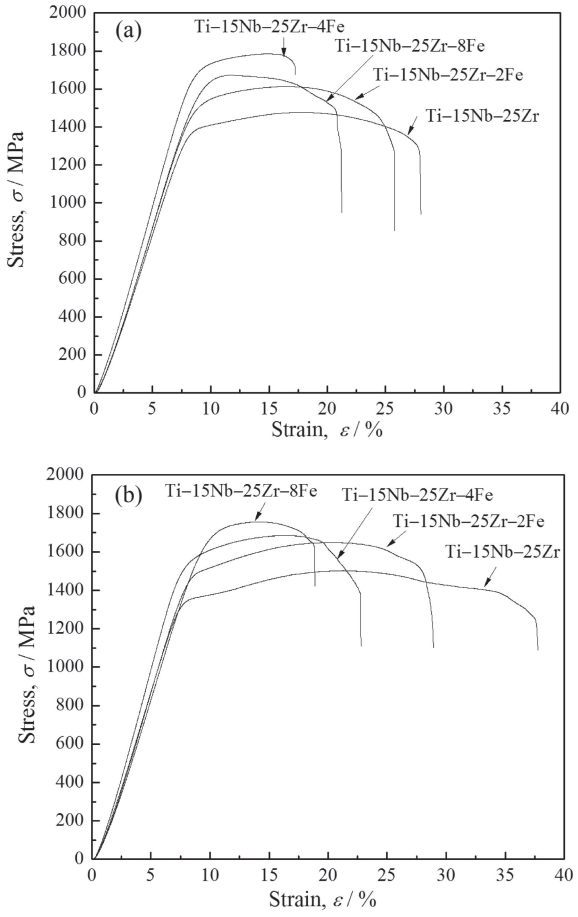

Fig. 7 Compressive stress–strain curves of the (a) as-sintered and (b) heat-treated Ti–15Nb–25Zr–(0, 2, 4, 8)Fe obtained at room temperature.

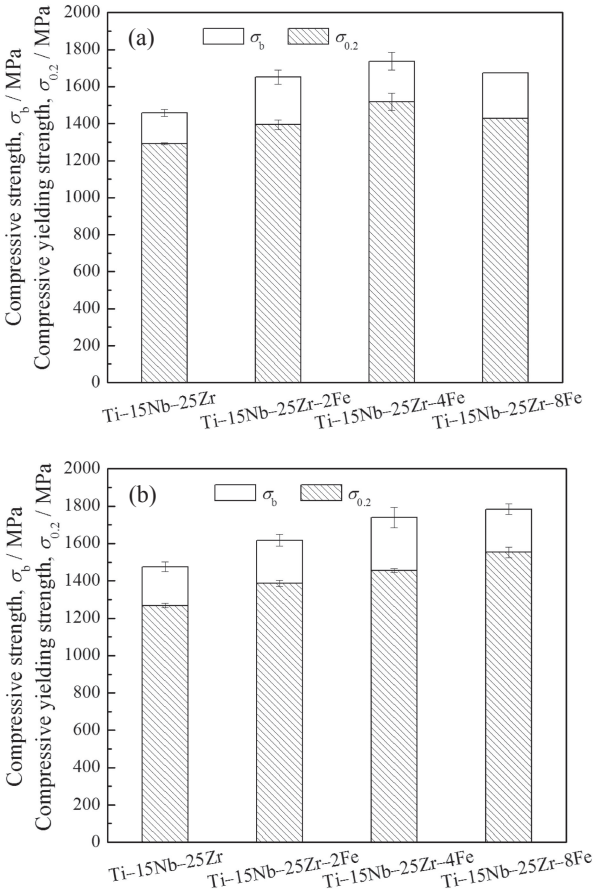

Fig. 8 Compressive strengths and yielding strengths of the (a) as-sintered and (b) heat-treated Ti–15Nb–25Zr–(0, 2, 4, 8)Fe alloys.

compressive stress–strain curves, the plasticity exhibits an opposite trend to that of σ_b. Among the as-sintered specimens, Ti–15Nb–25Zr–4Fe exhibits the shortest stress plateau (approximately 8%), which is still a good plasticity.

After the heat treatment, σ_b and $\sigma_{0.2}$ of Ti–15Nb–25Zr–(0, 2, 4)Fe are approximately equal to those of the as-sintered samples, but their plasticities are significantly increased. Ti–15Nb–25Zr–8Fe exhibits an increase in strength and decrease in plasticity. For Ti–15Nb–25Zr–(0, 2, 4)Fe, only small changes in XRD patterns and microstructures are observed between the structures before and after the heat treatment, as shown in Figs. 1, 2, 3, and 5. Therefore, the elemental diffusion in Ti–15Nb–25Zr–(0, 2, 4)Fe is not significantly improved by the heat treatment. However, the disappearance of intermetallic compounds in Ti–15Nb–25Zr–8Fe after the heat treatment (Fig. 2) indicates that element diffusion is promoted by the heat treatment. The solid-solution hardening becomes significant and the compressive strength in the as-sintered Ti–15Nb–25Zr–8Fe is significantly increased by the heat treatment, but its plasticity is decreased. The heat-treated Ti–15Nb–25Zr–8Fe also exhibits good comprehensive mechanical properties including a compressive strength of 1780 MPa and stress plateau of approximately 8%.

3.5 Discussion

Ball milling is usually carried out for mixing raw element powders to obtain mechanical alloying before sintering.[27] In this study, the powders are only mechanically mixed by a V-type mixing machine. Although ball milling is supposed to promote the uniform distribution of elements, single β phase is hardly obtained in some β-Ti alloys prepared by SPS.[25] Wen *et al.* also reported some segregation of Nb in Ti–26Nb–5Ag, although the powder was subjected to ball milling.[26] Therefore, the complete solution of alloying elements is hardly achieved by SPS, as the short sintering time is inadequate for the full diffusion of elements. However, the partial solution was sufficient to obtain the dominant β phase in the specimens prepared by SPS in this study and Ref. 31. Samples prepared by SPS exhibit higher microhardnesses than those of melted samples.[25,32] Although the microhardnesses of the studied as-sintered and heat-treated Ti–15Nb–25Zr–4Fe are relatively high (approximately 400 HV), they are lower than those of Ti–20Nb–13Zr and Ti–35Nb–7Zr–5Ta (mass%) prepared by ball milling and SPS (660 and 531–668 HV, respectively).[25,27] This can be explained as grain refinement and formation of nanocrystals in the powders can be obtained by ball milling. However, Ti–15Nb–25Zr–(0, 2, 4)Fe exhibit similar compressive strengths to that of Ti–35Nb–7Zr–5Ta.[25] It is worth noting that Ti–15Nb–25Zr–(0, 2, 4)Fe exhibit good plasticities, whereas Ti–26Nb–5Ag exhibits a brittle fracture.[26] We believe that local element diffusion also occurs in the specimens prepared by SPS without ball milling. The elemental distributions in the specimens are satisfactory to obtain high strengths and good plasticities.

According to the above results, Fe can stabilize the β phase and provide an effective solid-solution strengthening in the Ti–Nb–Zr alloys prepared by SPS. Although it is supposed that the heat treatment at 900°C for 1 h can promote the diffusion of the constituent elements, the obtained results show that the segregation of Nb still exists. The strengths of Ti–15Nb–25Zr–(0, 2, 4)Fe did not significantly change upon the heat treatment; however, their plasticities were considerably improved. A considerable increase in strength is obtained in the heat-treated Ti–15Nb–25Zr–8Fe with a decreased plasticity compared to those of the as-sintered sample. Therefore, the short heat treatment after the SPS is beneficial to improve the comprehensive mechanical properties. The as-sintered Ti–15Nb–25Zr–4Fe and heat-treated Ti–15Nb–25Zr–(4, 8)Fe exhibit good compressive mechanical properties including high hardnesses, high strengths, and good plasticities.

4. Conclusion

Ti–15Nb–25Zr–(0, 2, 4, 8)Fe were prepared by SPS from the mixture of pure element powders; some of them were subsequently heat-treated at 900°C for 1 h. Their microstructures and mechanical properties were analyzed. The following conclusions can be summarized:

(1) Both β and α'' phases existed in the as-sintered Ti–15Nb–25Zr–(0, 2, 4, 8)Fe. In addition, intermetallic compounds were detected by XRD in the as-sintered Ti–15Nb–25Zr–8Fe owing to the insufficient diffusion of the alloying elements. Segregation of Nb was observed in all of the alloys, which could not be completely eliminated by the heat treatment at 900°C for 1 h.

(2) The compressive strength and micro-Vickers hardness of the as-sintered Ti–15Nb–25Zr were increased by adding Fe (up to 4 mol%). The compressive strength had the highest value of 1740 MPa for the as-sintered Ti–15Nb–25Zr–4Fe, which decreased to 1670 MPa for the as-sintered Ti–15Nb–25Zr–8Fe. After the heat treatment, the plasticities of Ti–15Nb–25Zr–(0, 2, 4)Fe were increased, while the high compressive strengths were maintained. Ti–15Nb–25Zr–8Fe exhibited a considerable increase in compressive strength.

(3) High compressive strengths, high hardnesses, and good plasticities were obtained for the as-sintered Ti–15Nb–25Zr–4Fe and heat-treated Ti–15Nb–25Zr–(4, 8)Fe. These results suggest that SPS is a promising rapid fabrication method for high-performance β-Ti alloys and that the subsequent short heat treatment can improve the comprehensive mechanical properties.

Acknowledgement

This work was partially supported by the Natural Science Foundation of Shanghai, China (No. 15ZR1428400), Shanghai Key Technology Support Program (No. 16060502400), National Natural Science Foundation of China (No. 61504080), the project of Creation of Life Innovation Materials for Interdisciplinary and International Researcher Development, Tohoku University, Japan sponsored by Ministry, Education, Culture, Sports, Science and Technology, Japan, and the Grant-in Aid for Scientific Research (B) (No. 17H03419) from Japan Society for the Promotion of Science (JSPS), Tokyo, Japan.

REFERENCES

1) L.Q. Wang, Z.J. Lin, X.T. Wang, Q.W. Shi, W.Q. Yin, D. Zhang, Z.T. Liu and W.J. Lu: Mater. Trans. **55** (2014) 141–146.
2) L.C. Zhang and H. Attar: Adv. Eng. Mater. **18** (2016) 463–475.
3) Y.P. Peng, C.P. Ju and J.H.C. Lin: Mater. Trans. **59** (2018) 734–740.
4) Y. Liu, K.Y. Li, T. Luo, M. Song, H. Wu, J. Xiao, Y.N. Tan, M. Cheng, B. Chen, X.R. Niu, R. Hu, X.H. Li and H.P. Tang: Mater. Sci. Eng. C **56** (2015) 241–250.
5) S. Ehtemam-Haghighi, K.G. Prashanth, H. Attar, A.K. Chaubey, G.H. Cao and L.C. Zhang: Mater. Des. **111** (2016) 592–599.
6) Y.Y. Li, L.M. Zou, C. Yang, Y.H. Li and L.J. Li: Mater. Sci. Eng. A **560** (2013) 857–861.
7) L.C. Zhang, D. Klemm, J. Eckert, Y.L. Hao and T.B. Sercombe: Scr. Mater. **65** (2011) 21–24.
8) T. Shiraishi, K. Yubuta, T. Shishido and N. Shinozaki: Mater. Trans. **57** (2016) 1986–1992.
9) M.T. Mohammed: Karbala Int. J. Modern Sci. **3** (2017) 224–230.
10) P.F. Chui: Vacuum **143** (2017) 54–58.
11) A.L.R. Ribeiro, R.C. Junior, F.F. Cardoso, R.B.F. Filho and L.G. Vaz: J. Mater. Sci. Mater. Med. **20** (2009) 1629–1636.
12) V.A.R. Henriques, E.T. Galvani, S.L.G. Petroni, M.S.M. Paula and T.G. Lemos: J. Mater. Sci. **45** (2010) 5844–5850.
13) Z.M. Li, B.L. Zheng, Y.T. Wang, T. Topping, Y.Z. Zhou, R.Z. Valiev, A. Shan and E.J. Lavernia: J. Mater. Sci. **49** (2014) 6656–6666.
14) Z.Y. He, L. Zhang, W.R. Shan, Y.Q. Zhang, Y.H. Jiang, R. Zhou and J. Tan: Acta Metall. Sin. (Engl. Lett.) **29** (2016) 1073–1080.
15) Y. Cui, Y. Li, K. Luo and H.B. Xu: Mater. Sci. Eng. A **527** (2010) 652–656.
16) S. Ozan, J.X. Lin, Y.C. Li, Y.W. Zhang, K. Munir, H.W. Jiang and C.E. Wen: J. Mech. Behav. Biomed. Mater. **78** (2018) 224–234.
17) Q. Li, M. Niinomi, M. Nakai, Z.D. Cui, S.L. Zhu and X.J. Yang: Mater. Sci. Eng. A **536** (2012) 197–206.
18) J.M. Calderon Moreno, C. Vasilescu, S.I. Drob, E.I. Neascu and M. Popa: Mater. Corros. **65** (2014) 703–714.
19) S.L. Chen: Shanghai Nonferrous Metals **35** (2014) 47–52.
20) A. Zafari, Y.P. Ding, J.Z. Cui and K.N. Xia: Metall. Mater. Trans. A **47** (2016) 3633–3648.
21) S.K. Vajpai, M. Ota, T. Watanabe, R. Maeda, T. Sekiguchi, T. Kusaka and K. Ameyama: Metall. Mater. Trans. A **46** (2015) 903–914.
22) D.J. Wang, H. Yuan and J.M. Qiang: Metals **7** (2017) 207.
23) R. Yamanoglu, W. Bradbury, E.A. Olevsky and R.M. German: Met. Mater. Int. **19** (2013) 1029–1034.
24) R. Yamanoglu, W. Bradbury, E. Karakulak, E.A. Olevsky and R.M. German: Powder Metall. **57** (2014) 380–386.
25) L.M. Zou, C. Yang, Y. Long, Z.Y. Xiao and Y.Y. Li: Powder Metall. **55** (2012) 65–70.
26) M. Wen, C. Wen, P. Hodgson and Y. Li: Mater. Des. **56** (2014) 629–634.
27) M.A. Hussein, C. Suryanarayana and N. Al-Aqeeli: Mater. Des. **87** (2015) 693–700.
28) W.F. Ho, C.H. Pan, S.C. Wu and H.C. Hsu: J. Alloys Compd. **472** (2009) 546–550.
29) B.B. Zhang, B.L. Wang, Y.B. Wang, L. Li, Y.F. Zheng and Y. Liu: J. Biomed. Mater. Res. Part B **100B** (2012) 185–196.
30) J.L. Murray: *ASM Handbook, Volume 3 Alloy Phase Piagram*, ed. by H. Baker and H. Okamoto, (ASM International, Electronic Vision, 1998) pp. 1194 & 1572.
31) Z.Y. He, L. Zhang, W.R. Shan, Y.Q. Zhang, R. Zhou, Y.H. Jiang and J. Tan: Trans. Nonferrous Met. Soc. China **27** (2017) 848–856.
32) E.B. Taddei, V.A.R. Henriques, C.R.M. Silva and C.A.A. Cairo: Mater. Sci. Eng. C **24** (2004) 683–687.